Catena 225 (2023) 107016

Contents lists available at ScienceDirect

Catena

journal homepage: www.elsevier.com/locate/catena

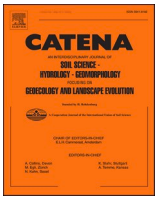

Where does a glacier end? Integrated geophysical, geomorphological and photogrammetric measurements to image geometry and ice facies distribution

I. Santin [a,*], E. Forte [a], M. Nicora [b], S. Ponti [b], M. Guglielmin [b,c]

[a] Department of Mathematics and Geosciences, University of Trieste, via Weiss, 2, 34128 Trieste, Italy
[b] Department of Theoretical and Applied Sciences, Insubria University, via Dunant, 3, 21100 Varese, Italy
[c] Climate Change Research Center, Insubria University, Via San Abbondio, 22100 Como, Italy

ARTICLE INFO

Keywords:
Debris covered glaciers
GPR
Photogrammetry
Dead ice
Glacier monitoring

ABSTRACT

In this study we integrated different techniques, spanning from Ground Penetrating Radar to geomorphological and photogrammetric data, to characterize the glacial and proglacial environments of the Sforzellina Glacier (Central Alps, Italy). Direct data highlighted the presence of debris-covered ice and even of dead ice patches in front of the actual glacier terminus. Such an information was further proved by geophysical data. We try to correlate the dead ice patches occurrence with several parameters such as debris cover thickness, ground temperature, solar radiation, elevation, velocity of glacier retreat, and dip of the topographic surface without finding relevant correlations, except for the local bedrock morphology. In fact, the latter factor seems to be crucial to make the favourable conditions to dead ice patches formation and preservation with time.

Since ice is not always outcropping, while dead ice patches never outcrop because they are hidden by continuous debris cover, classical glaciological monitoring techniques are not always successfully applicable.

On the basis of the obtained results, we argue that estimates of glacier extension just related to surficial information, like in the case of exclusive use of remote sensing data and outcropping ice monitoring, can produce relevant underestimations. The presence of hidden ice patches, even not strictly part of the glacier body, is further important to quantify the total water equivalent, as well as to make affordable forecasts of the future glaciers evolution.

1. Introduction

Worldwide recession of glaciers is one of the clearest evidences of global warming (Paul et al. 2007, IPCC, 2021). Accurate mapping and monitoring the evolution in time of ice bodies are therefore essential for assessing the impacts of the changing climate on the global extent of glaciers. The evaluation of the total ice mass, and, consequently, of the water storage, requires a precise and accurate reconstruction of glaciers geometry, especially for what concerns their volume, in order to infer realistic forecasts of their future evolution. Considering that mountain glaciers represent a challenging environment from the logistical point of view, numerous techniques based on remote sensing were implemented for glaciers extent mapping (Paul et al., 2013), exploiting both manual (Bernard et al., 2014) and automated methods (Paul et al., 2003). However, the presence of surficial debris represents a highly-challenge issue for evaluating the actual glaciers extent by only exploiting remote sensing data, especially in the case of debris-covered glaciers. The actual extent and glaciers termini below the debris cover in turn affect the proper evaluation of the accumulation area to total area of the glacier (AAR) which is essential to calculate the equilibrium line altitude (ELA), thus misleading the assessment of glaciers health. The ELA marks the altitude where the climatic mass balance equals to zero at a given time and monitoring its evolution is one of the methods to quantify the response of ice bodies to a changing climate (Žebre et al., 2021). According to Anderson et al. (2018), debris-covered glaciers are the middle term of a debris-involving ice masses continuum, in which debris added to the glacier surface in the accumulation area then follows an englacial path until the point of emergence in the ablation zone. The properties and transport of debris and its direct effect on the surface insulation have been well studied e.g. by Huo et al. (2021) and modelled by Anderson

* Corresponding author.
E-mail address: ilaria.santin@phd.units.it (I. Santin).

https://doi.org/10.1016/j.catena.2023.107016
Received 18 November 2022; Received in revised form 12 January 2023; Accepted 12 February 2023
Available online 21 February 2023

and Anderson (2016), concluding that debris-covered glaciers still represent a complex and challenging environment to be investigated. The thickness of the debris cover, depending by several factors including structural and morphological characteristics of the surroundings (Dobreva et al., 2017; Mayr and Hagg, 2019; Draebing, 2021; Tarca and Guglielmin, 2022) determines the amount of ice melting (Giese et al., 2021) as debris enhances or limits ice ablation. The latter process is in turn responsible for downstream impacts such as freshwater availability, hydroelectric power generation, natural hazards, and landscape evolution (Immerzeel et al., 2010; Bush et al., 2020). As debris cover conceals the glacier limit, it also could hide stagnant glacial ice patches, referred as *dead ice*, for which downward glacier flow movements have ceased (Benn and Evans, 2010). Remnant dead ice can occur during the shrinking of a glacier, while glacier snout retreats and debris cover often accumulates on the surface (Schomacker, 2007). In addition, it is further associated to permafrost areas and ice-cored landforms, as responsible for hummocky moraine development (Krüger et al., 2010). Dead ice below debris cover areas can be identified by direct measurements as ice cores in specific locations (Henriksen et al., 2003) and by means of geophysical methods (Ribolini et al., 2010; Onaca et al., 2022), which have already proved their effectiveness in identifying hidden dead ice patches (Yoshikawa et al., 2006).

In this study we exploit the integration of different techniques, spanning from Ground Penetrating Radar (GPR) surveys to geomorphological and photogrammetric data analyses, in order to characterize the glacial and proglacial environments of the Sforzellina Glacier (Central Alps, Italy) estimating the actual boundary of the glacial body not limiting it to the zones with outcropping ice. In addition, we also considered hidden ice patches that cannot be even supposed just from remote sensed datasets, while integrated direct and geophysical measures can address this issue and image both outcropping and hidden ice facies. We further compared the inferred dead ice distribution with debris cover thickness, ground temperature, solar radiation, elevation, velocity of glacier retreat, and slope of the topographic surface in order to analyse possible correlations with the setting of the study area.

2. Study area

The Sforzellina Glacier (46°20′55″ N, 10°30′50″ E) is located on the right-hand side of the upper Gavia Valley within the Stelvio National Park, Italy. (Fig. 1). It is cirque glacier that can be actually considered as a debris-covered glacier as its surface is covered by supraglacial debris for the 66.8 % of the total glacier extension, with a debris accumulation rate equal to 621 g/m^2 per day, as calculated by *Tarca and Guglielmin (2022)*. The glacier lies on the north-western side of the Corno dei Tre Signori (3360 m a.s.l.) and the surroundings are mainly characterized by micaschists, paragneiss and orthogneiss outcrops (Montrasio et al., 2012). The glacier forefield is marked by complex morainic ridges which testify the retreat of the glacier front since the Little Ice Age (Guglielmin et al., 1995). The recent areal and volumetric shrinking is well documented by Cannone et al. (2008) between 1986/87 and 2006 with an acceleration of the mass lost after 2000 from 300,000 to 500000 m^3/yr w.e. The retreat is still ongoing and the glacier area reduced from about 0.4 km^2 (Pavan et al., 2000) to 0.22 km^2 in 2016 (Paul et al., 2019). Several geophysical surveys were performed on the glacier surface, starting from Resnati and Smiraglia (1989) with Vertical Electrical Surveys (SEV), revealing ice thicknesses in specific locations equal to 15 m (accumulation zone), 30 m (glacier central body) and 8 m (ablation area). In 2000 Pavan et al. (2000) performed another geophysical survey, applying both reflection seismic and GPR measurements. The integration of these techniques allowed to obtain more detail estimates of the ice thickness and the bedrock morphology, revealing a maximum ice thickness of 60 m and highlighting overthrusting and foliation of the ice in the ablation zone and apparent bedrock overdeepening.

Considering the current climatic evolution, which is responsible for both the increasing rate of supraglacial debris accumulation and the simultaneous retreat of the snout, the Sforzellina Glacier can be considered a debris-covered glacier that could be develop into a rock glacier, thus reaching the final term of the debris-ice involving continuum, as described by Anderson et al. (2018).

3. Methods

3.1. Remote sensing

3.1.1. Photogrammetric and thermal surveys

Two unmanned aerial vehicle (UAV) photogrammetric surveys were conducted in September 2021 at the maximum melting of the glacier, in different moments of the day. We used a DJI Matrice 210 drone with a Real Time Kinematic (RTK) antenna, able to guarantee a 2 cm vertical precision of the geotags. The flight surveys consisted in a nadiral acquisition of the images, all of them taken at a constant elevation of 130 m above the ground. The camera used at the first survey was a DJI Zenmuse X5s with a 12 mm lens that acquired RGB images at 20.8 MP. A total of 882 images were taken, assuring an overlap of at least 60 % in x and y directions. Afterwards, a bundle adjustment of the images was run in Agisoft Metashape 1.8 in order to obtain the digital terrain model (DTM) and orthophoto of the area.

The camera used for the second survey was a DJI Zenmuse XT2; it is a thermal sensor with a 19 mm lenses that acquired 672 thermal images of 640 × 512 pixels (0.1 °C of resolution, 2.0 °C of absolute accuracy). Despite the poorer overlap of thermal images compared to RGB images

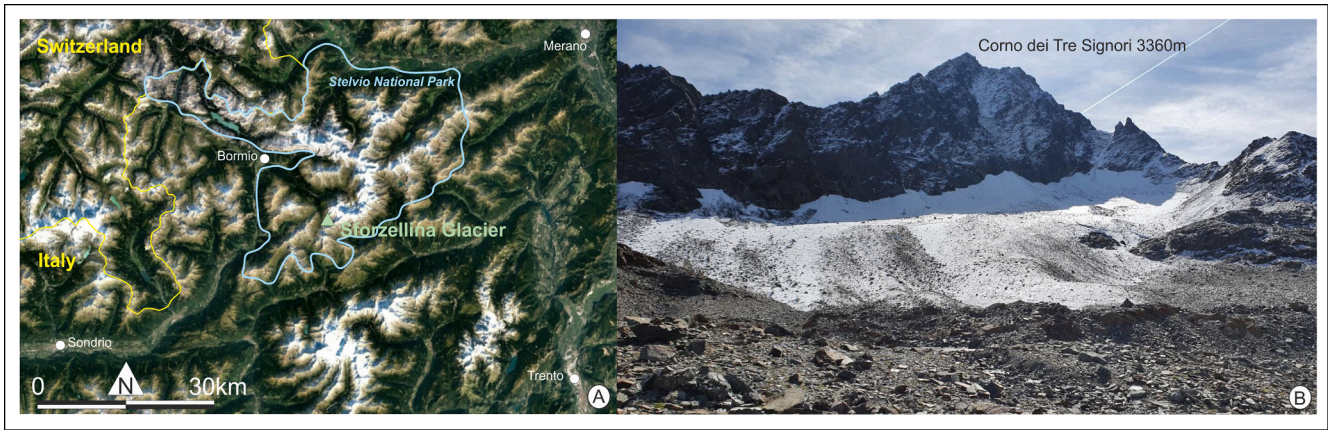

Fig. 1. (A) Location map of the study area. (B) Photograph of the Sforzellina Glacier taken in September 2021 during the geophysical survey highlighting the amount of surficial debris covering most of the glacier surface.

(<50 %), we made a Structure from Motion bundle adjustment in Agisoft Metashape 1.8, thus obtaining a thermal orthophoto of the entire glacier, similarly to Forte et al. (2021). The obtained surface temperatures were calibrated by setting to 0 °C the surface temperature of the snow patches (in presence of positive air temperatures during the survey). In this way, it was possible to increase the measurement accuracy, independently from the adopted emissivity value (Kraaijenbrink et al., 2018).

3.1.2. GIS analysis

The RGB orthophoto was imported in ArcGIS 10.8 and the limit of the visible glacier ice of September 2021 was visually delineated (Fig. 2). The same procedure was conducted on orthophotos of different years (1998, 2003, 2007, 2012, 2015) downloaded from the regional topographic service (https://www.geoportale.regione.lombardia.it/) in order to visually mark the visual glacier terminus changes in time. The 1984–1985 limit of the glacier terminus was instead extracted from Cannone et al. (2008). It represents the last glacier advance, hereafter referred as "1984".

3.2. Debris thickness direct measurement

The debris thickness was measured in the field in selected points through direct excavations down to the visible glacier ice surface or, in any case, down to a maximum depth of 60 cm where no glacier ice had been detected. Such measurements were carried out along several transects starting from the glacier ice exposed surface and moving downward with a span equal to 5 m.

3.3. Geophysics

Geophysical methods are widely applied in glaciology (Godio, 2019) and Ground Penetrating Radar (GPR) is one of the most exploited thanks to its high efficiency in glacial environments, and high achievable resolution (Navarro and Eisen, 2009). GPR has proved to be effective in providing detailed imaging of the internal structure of glaciers (Forte et al., 2021) as well as to characterize different frozen materials (Godio and Rege, 2015) and glaciological features at different scale levels (Arcone, 1996, Colombero et al., 2019, Church et al., 2021). GPR method bases on the transmission of electro-magnetic (EM) waves and on the registration of travel-time and amplitude of the reflections generated at the EM impedance contrasts between different materials (Jol, 2009).

A ground-coupled GPR survey was performed in September 2021 on the Sforzellina Glacier, resulting in a 2 km-long dataset of GPR profiles, located both outside and inside the debris-covered glacier boundary (Fig. 2). Survey was carried out with a ProEx (Malå Geoscience) GPR system, equipped with 250 MHz shielded antennas, triggered by an electro-mechanical odometer, obtaining a constant trace interval equal to 0.10 m. Trace positioning was guaranteed by a differential GPS device (Magellan Promark II) with a dm location accuracy. Despite the good quality of the raw GPR data, processing was essential to increase the signal/noise ratio thus improving the overall imaging, while maintaining the original data signature and preserving the amplitude contrasts essential for the characterization of EM facies. An EM facies can be defined as a portion of a GPR profile (or volume) characterized by a similar response to the EM signal. In fact, each material responds to the EM wave propagation in a peculiar way, which is related to its physical, chemical and even geometrical properties. The dataset was processed using Prism Software (Radar System Inc.) as well as some in-house modules implemented in Python. The processing flow includes drift removal (zero-time correction), bandpass filtering (corner frequencies are 20–80–250–650 MHz), background removal, exponential amplitude recovery, topographic (static) correction and depth conversion. For the last step, we considered a velocity value equal to 17 cm ns^{-1} for outcropping ice and to 13 cm ns^{-1} for materials below the glacier, on the basis of dedicated diffraction hyperbolas analyses. Table 1 shows the relation between the depth [cm] of the base of debris and the two-way travel time [ns] of the corresponding horizon in the GPR profiles at the same locations. From such validation points, we obtained a mean EM velocity equal to 10 cm ns^{-1}. Calibration points on the glacier surface cannot be used for velocity estimation because the debris thickness was

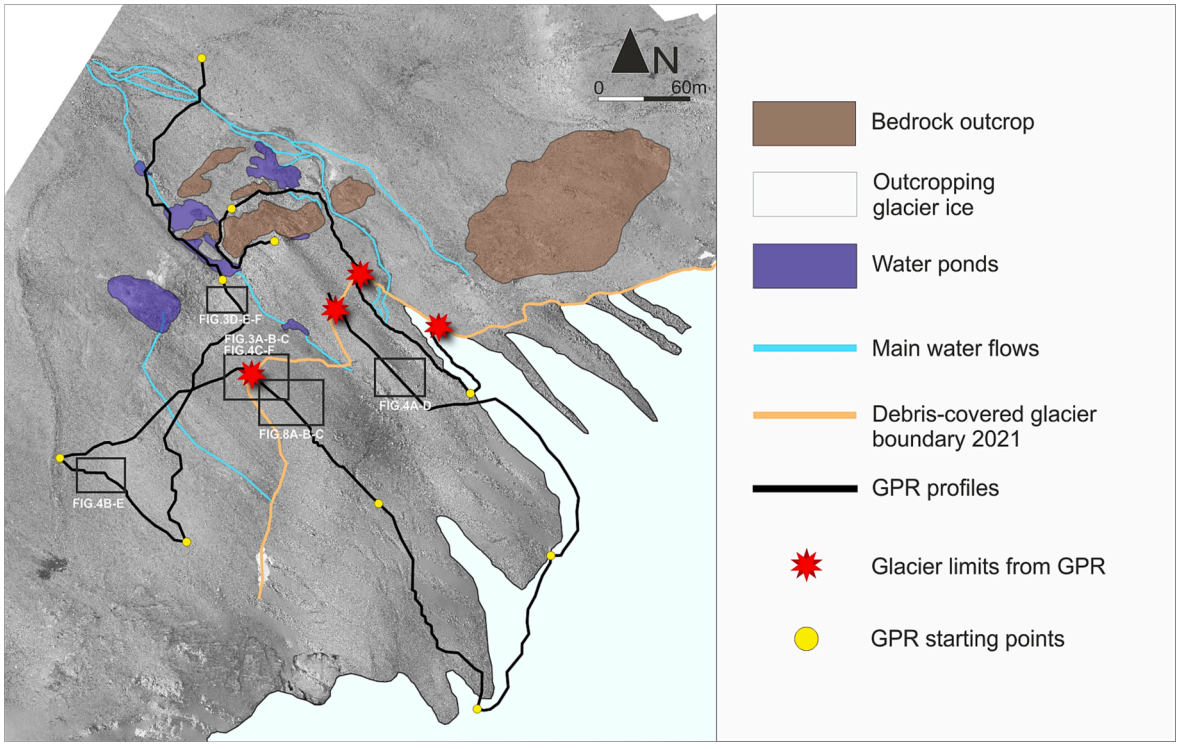

Fig. 2. Orthophotos mosaicking (September 2021) with superimposed: outcropping bedrock and glacier ice areas; water ponds and main water flows; GPR profiles location; inferred debris-covered glacier boundary (from integrated 2021 GPR and geomorphological surveys). Locations of Fig. 3,4 and 8 are also indicated.

Table 1
Relation between the depth of the base of debris and the two-way travel time of the corresponding horizon in the GPR profiles.

Calibration Points	*Debris thickness [cm]*	*TWT [ns]*	*Velocity [cm ns^{-1}]*
GPR Profile 5729			
	60	11.91	11.0
	60	12.28	9.8
	60	12.65	9.5
GPR Profile 5731			
	20	4.05	10.0

therein lower than the maximum optical resolution limit of a 250 MHz antenna, equal to a quarter of wavelength and corresponding to about 15 cm for the above EM velocities. Therefore, on GPR profiles located where the glacier is covered by debris, the base of the surficial debris cannot be identified on GPR profiles since its reflection interferes with the direct ground wave. GPR interpretation was supported by GPR attribute analysis, which allowed to better image and understand the boundaries and the geometries of the EM facies and horizons on GPR profiles. GPR attributes are defined as any component extracted from geophysical data that can be analysed in order to enhance hidden information (Chopra and Marfurt, 2005). Similarly to seismic attributes (calculated on reflection seismic data), GPR attributes can emphasize peculiar signal characteristics related, for instance, to the phase continuity, frequency content, texture pattern, attenuation behaviour, among the others. GPR attributes are used in different fields and with different objectives, such as archaeology (Pipan et al., 2001; Zhao et al., 2018), environmental analyses (Kadioğlu and Kadioğlu, 2016), structural geology (McClymont et al., 2008; Ercoli et al., 2015) automated reflectors picking (Dossi et al., 2015), while examples of application of GPR attributes in glaciology can be found in Zhao et al. (2016) and Lu et al. (2020). We here exploit amplitude-, phase- and frequency-related attributes, to obtain improved imaging and a better facies assessment. Phase-related attributes, as the cosine of instantaneous phase, allow to highlight the horizon continuity even in zones with low signal-to-noise ratio, providing a more constrained and effective interpretation. Therefore, horizons interpretation was performed by seeded 2D auto tracking functions applied on the cosine of instantaneous phase attribute, obtaining a mean travel time uncertainty equal to 1.50 ns, i.e. half phase. Such value corresponds to a length equal to about 15 cm when considering the mean velocity of 10 cm ns^{-1} previously obtained by direct calibrations. Manual picking was limited to the portions of some reflectors with low phase continuity and where interfering event were present. Also, we calculated and imaged the sweetness composite attribute, which is a complex attribute defined as the ratio between the instantaneous amplitude and the square root of the instantaneous frequency. Such attribute favours the detection of the boundaries between zones having different EM characteristics. Dominant frequency attribute is an instantaneous attribute marking the frequency with the highest amplitude for each trace sample.

4. Results and discussions

At first, we analysed all the GPR profiles crossing both the

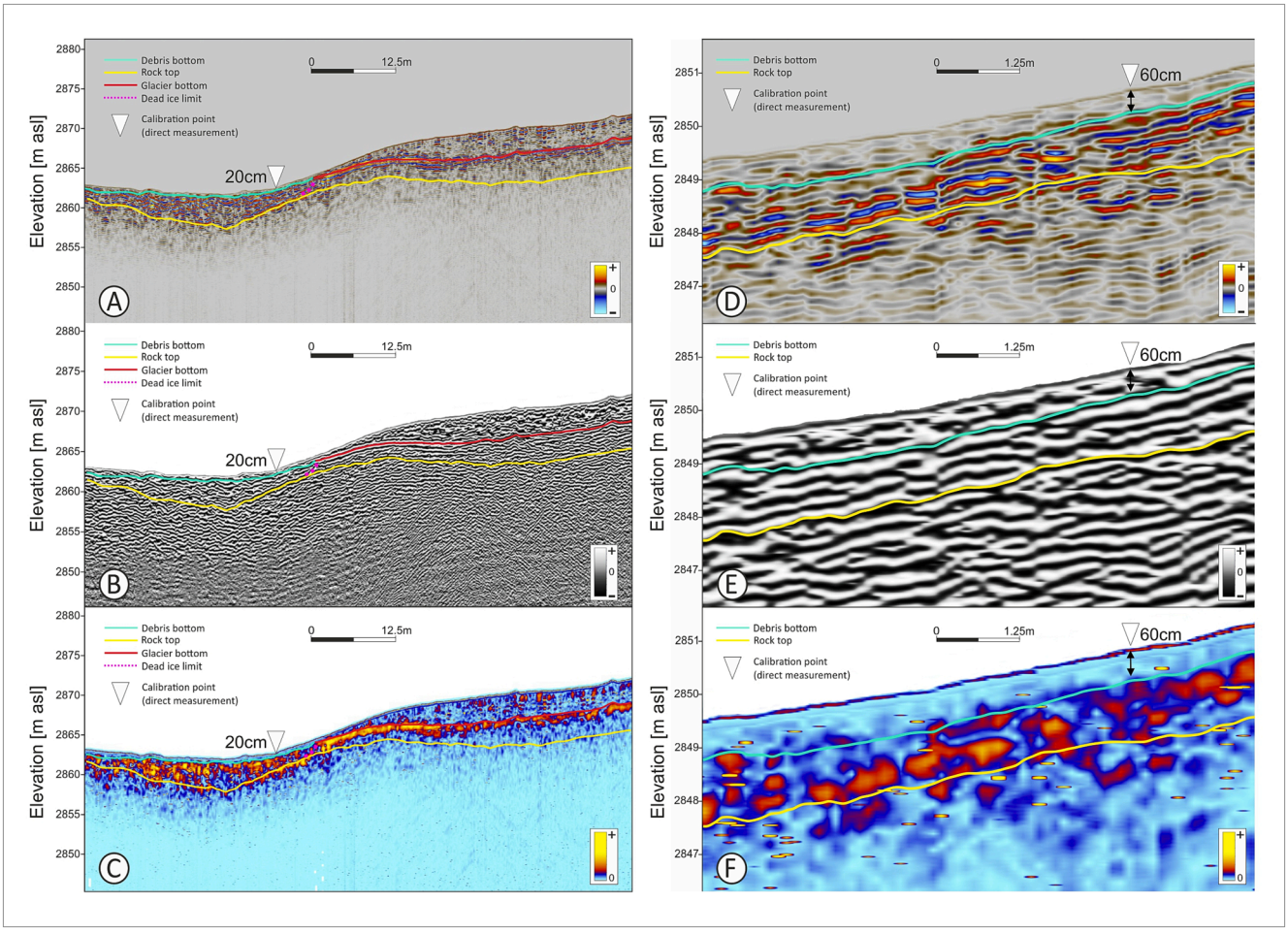

Fig. 3. GPR exemplary data (A, D) and their cosine of instantaneous phase (B, E) and sweetness (C, F) attributes displays. White arrows mark the direct thickness measurements locations used as thickness cross-validation points. See text for horizons interpretation details.

outcropping glacier ice, the debris-covered glacier, as well as the glacier forefield (Fig. 2), calibrating the debris thickness with direct measurements (Fig. 3).

GPR attribute analysis supports the interpretation of horizons and in particular their actual location and lateral continuity. As a matter of fact, both phase-related (cosine of instantaneous phase in Fig. 3B-E) and composite (sweetness in Fig. 3C-F) attributes point out different components of the GPR data, which, once combined, allowed a more detailed imaging of the internal structure of the Sforzellina glacier and forefield. In particular, the cosine of instantaneous phase allowed a more constrained interpretation of both debris bottom, rock top and glacier bottom reflections (Fig. 3B-E), while the sweetness attribute enhances the signature of different reflection amplitude zones, such as debris cover, dirty and clean ice. Clean (i.e. with low impurities) ice is generally displayed as an EM transparent facies, due to its quite homogeneous composition, while its low overall electrical conductivity allows the EM signal to propagate downward without relevant attenuation. In case of local impurities as debris particles, scattering phenomena can occur depending by the signal frequencies and debris size ratio, resulting in a facies characterized by no clear reflections and by isolated diffraction hyperbolas. Furthermore, we recognized some high amplitude quite continuous reflections in between the transparent facies: they are reasonably related to debris levels within the glacier. In Fig. 4A and D, it is apparent that in the Sforzellina glacier there are two domains, namely: massive relatively clean ice toward the glacier's top and dirty ice with local strongly thickly layered internal debris toward the front having a mean thickness equal to about 2 m (dotted black line in Fig. 4A and D). The lateral limit between such two facies is very clear (dotted blue line in Fig. 4A and D) along all the profiles over the glacier (Fig. 2). Another facies has been identified at the base of clean ice, having less internal layering but higher scattering than the previous one: it can be reasonably associated to a mixture of basal debris with ice, likely a ground moraine. Basal debris lies directly above the metamorphic bedrock of the Sforzellina glacier, although the top of the bedrock is not always imaged on GPR profiles, especially when the basal debris is thicker (continuous or dotted yellow line). Clean ice, dirty ice, and basal debris facies are all involved in the glacier dynamics, being subjected to the downward movements of the glacier mass. However, in GPR profiles located in the northern glacier forefield, where the ice never outcrops, a mainly transparent additional GPR facies, with higher scattering than clean ice and local not continuous stratifications has been detected (Fig. 4B and E). Its upper boundary appears as a high-amplitude not always continuous reflection, which is an indicator of high electromagnetic impedance contrast between materials above and below the interface, as happens between sediments and ice. Four trenches, located in correspondence of GPR profiles, allowed to associate this facies with relict ice masses (i.e. *dead ice*), lying below a variable thickness debris cover. Therefore, such high-amplitude reflection actually corresponds to the interface between surficial debris and dead ice. As a matter of fact, direct data was essential for an unambiguous validation of the GPR facies interpretation, allowing to understand the dead ice facies characteristics. In particular, visual inspection of the trenches demonstrated

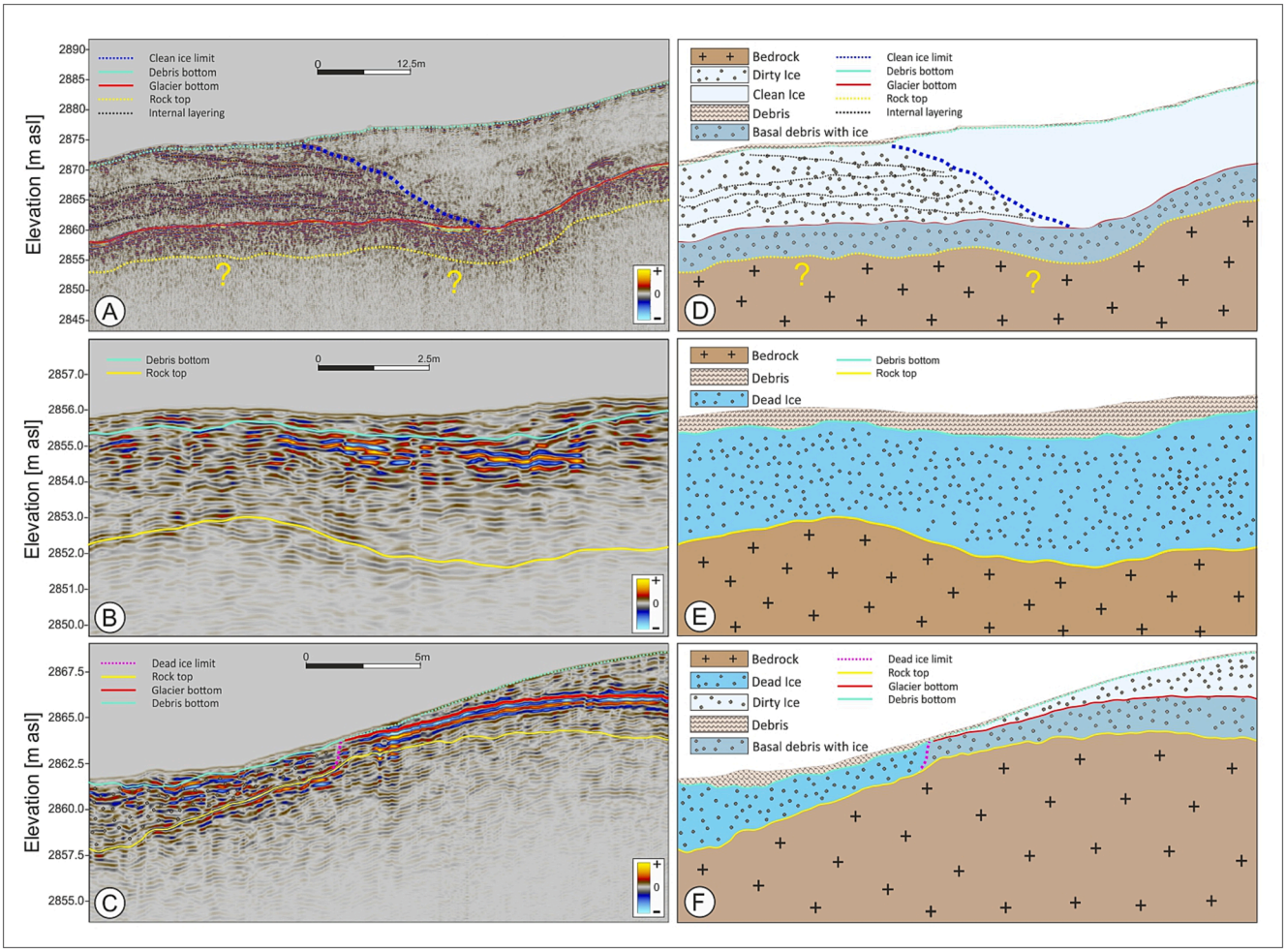

Fig. 4. GPR interpretation and glaciological facies/units schemes on three different peculiar zones of the glacier (see Fig. 2 lor location), namely: the transition between clean and dirty ice within the glacier (A, D); the ice free area North to the apparent glacier limits (B, E); the transitional zone centred on the glacier front (C, F). Please notice that the scales of profiles are different.

the presence of dead ice with debris below a debris cover with variable thickness (Fig. 5). The assessment of dead ice was also supported by GPR attributes analysis, especially by the sweetness one, which exhibits high values for the dead ice facies (Fig. 3C and F). The basal limit of the dead ice facies is imaged only where this layer is thin enough, due to the attenuation caused by the internal scattering strongly limiting the maximum penetration depth of the GPR signal. In Fig. 4C and F, dotted pink line marks the lateral contact between basal debris and dead ice.

Table 2 summarizes the main GPR characteristics of each interpreted and previously described GPR facies, in terms of signal amplitude, scattering, layering, and GPR attributes signature. Fig. 5 is the result of the integration among direct data, GPR survey and photogrammetry, showing the supposed extension of dead ice patches with the evolution of the glacier boundary since 1984, superimposed to the orthophoto collected in 2021 from the UAV. The integration of direct and indirect methods allowed to reconstruct in detail both the surficial features such as the past glacier boundaries, water ponds, water flows, and bedrock outcrops, as well as subsurface structures like dead ice patches extension, dirty ice limits, and the debris-covered glacier boundary. Glacier outlines from 1984 (with its frontal moraine) to 2021 (the last one provided by GPR data and marked by the orange line in Figs. 2, 5, 6, 7), highlight a not homogeneous retreat of the glacier front, exceeding 200 m in some locations in the considered time period, with the maximum withdraw between 2015 and 2021 in the central part of the glacier front. If we consider as the 2021 glacier limit the border of the outcropping ice (white patch in Figs. 2, 5, 6, 7) instead of the one inferred by 2021 GPR measurements, we obtain an overestimation of the glacier retreat up to over 450 m in the same 1984–2021 period. In fact, all the area where ice was not outcropping, but was detected by GPR, would not be considered as part of the 2021 glacial body. The minimum retreat was toward the west where most of the dead ice was detected. Two dead ice patches were identified along GPR profiles outside the debris-covered glacier boundary, one extending from the glacier terminus to the northern bedrock outcrops and water ponds, while the other has a south-western limit which cannot be determined as no coverage of GPR profiles was present in that zone. Considering that the dead ice patches are both located between the frontal moraine of 1984 and the debris-covered glacier front, they are most likely made by dead ice formed approximately in the last 40 years. As a matter of fact, it is apparent that dead ice occurrence is not correlated with velocity of the retreat of the Sforzellina Glacier. In addition, debris cover thickness does not affect the occurrence of dead ice, since it is both present below about 100 and only 20 cm of debris, even it can affect the dead ice resilience with time (Fig. 5).

Table 2
Summary of the GPR facies characteristics in terms of signal reflection amplitude, scattering, layering, attributes signature. DF (dominant frequency); PH (cosine of instantaneous phase); SW (sweetness).

GPR FACIES	*REFLECTION AMPLITUDE*	*SCATTERING*	*LAYERING*	*Attributes signature*
Clean ice	Very low (transparent)	No (or very localized)	No, except for shear zones	High DF; discontinuous PH; low SW
Dirty ice	Medium and discontinuous	Moderate	Local, quite continuous	Medium DF; locally continuous PH; medium SW
Basal debris with ice	High	Variable	Low to absent	Medium to low DF; locally continuous PH; high SW
Dead ice	High	High, locally variable	Only local	Medium DF; locally continuous PH; highest SW

Fig. 6 showed the comparisons among dead ice occurrences and topographic surface elevation, slope, and solar radiation, obtained from a digital terrain model collected from the 2021 photogrammetric UAV survey. Dead ice patches extend from about 2880 to 2850 m asl, spanning from west toward north-east. Although the topography has a difference in elevation of about 30 m, dead ice existence appears to be not driven by such an elevation interval. Same considerations are provided by the slope terrain analysis, as dead ice is located mostly on flat topography, even though locally there are some high-slope zones, reaching almost 40° (Fig. 6B). The analysis of the DTM confirms, as previously stated, that the debris-covered glacier boundary is not apparent just on the basis of the orthophotos and DTM because there are no abrupt changes in elevation and slopes between the outcropping ice and the debris covered ice zones. Fig. 6C depicts the incoming solar radiation, which allows to calculate the insulation considering the total amount of radiation as the sum of direct, diffuse, and global insolation.

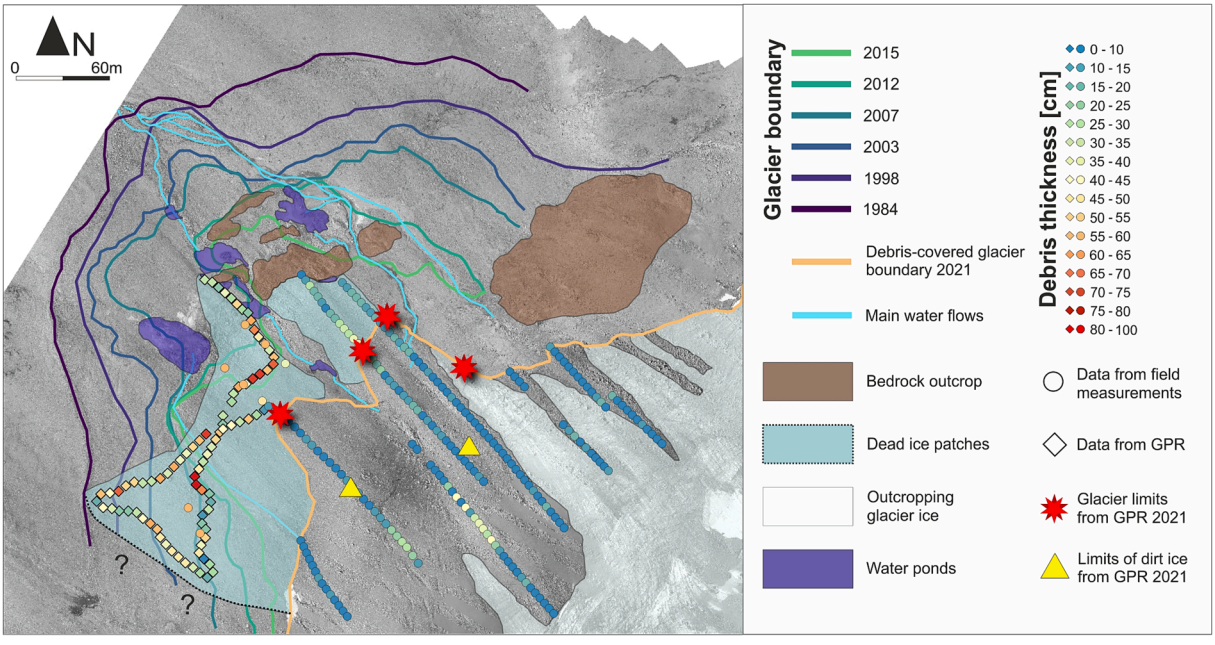

Fig. 5. Debris thickness above ice from both direct (circles) and GPR (squares) measurements and inferred extension of dead ice patches based on integrated data.

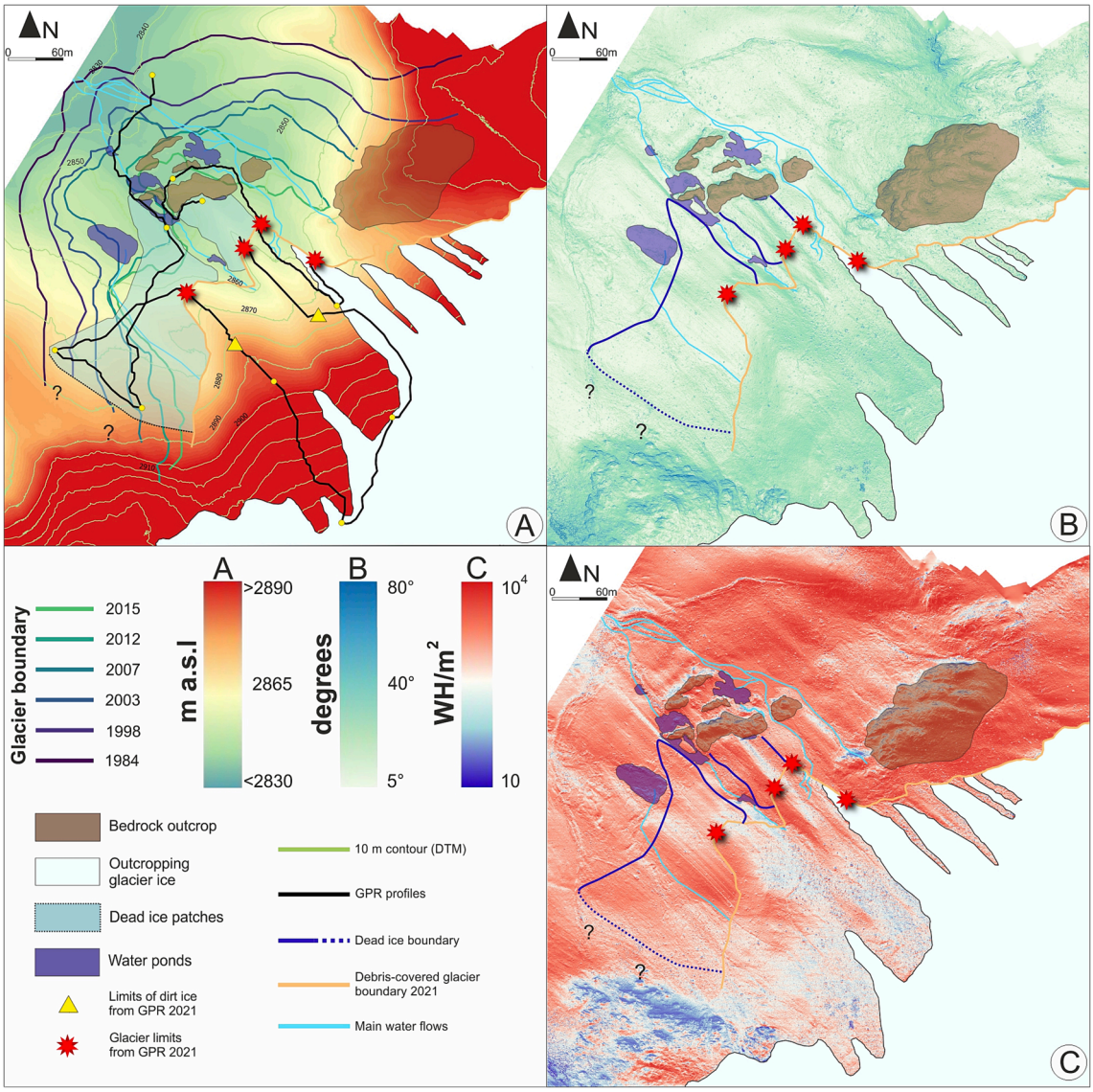

Fig. 6. DTM (A), terrain slope (B) and calculated solar radiation (C) from 2021 photogrammetric UAV survey with locations of: past glacier's snouts, GPR profiles, outcropping bedrock areas, water ponds, main flow paths, and the debris-covered glacier boundary from 2021 GPR survey.

Also in this case, the occurrence of dead ice has no clear correlation with specific solar radiation values.

Due to the steep rocky walls facing North and surrounding the accumulation zone of the Sforzellina Glacier, during the thermal UAV survey, most of the glacier was in shadow. Therefore, the thermography map in Fig. 7 showing the distribution of surficial temperatures, has a wide masked zone toward South-East. Secondary smaller masking has also been conducted on little portions of shadows caused by the uneven topography. Surficial temperatures distribution clearly discerns the actual Sforzellina Glacier (overall lower and close to zero temperatures) from the proglacial environment, where temperatures rise, reaching about + 10 °C. Although dead ice patches are all localised in the central zone where ground surface temperature was averagely + 5 °C, their extension spans over a very wide range of temperatures, thus suggesting no remarkable and evident correlations between surficial temperature and dead ice occurrence. As a matter of fact, the most extended dead ice patch subtends a minimum temperature in the south-west side equal to −4.2 °C, while in the northern part it reaches a maximum of 17.2 °C. This means that the surface temperature range for the larger and smaller dead ice areas is equal to 21.0 °C and 17.0 °C, respectively. Moreover, if one focuses only on this map, it seems to be unable to highlight water ponds and rocky outcrops, probably due to the contemporary presence of sunlight illuminated and shadow zones, as well as to peculiar effects on temperature of both debris size and surface aspect. The moraine ridge developed during the last advance of 1984 is clear, but it is just a visible effect of the variability of the aspect (see DTM in Fig. 6) that causes higher or lower temperatures.

Photogrammetric and thermal information is not always sufficient to define the actual glacier snout even when integrated with DTM data, as reported in Bernard et al. (2014) which shown that GPR surveys demonstrated the ice extends beyond the limits usually mapped for glaciers in their case study focused on the Austre Lovénbreen glacier in Svalbard. In our case, even though the visible outcropping glacier ice was well delimited for different years, the comparison between the 2021 terminus detected via GPR and orthophoto is largely diverse. We calculated the areal difference between the underestimated visual and the GPR limits: it is equal to 44940 m^2 being obviously larger including the dead ice patches. It is certainly true that by definition a glacier does not encompass dead ice (or even isolated ice patches) since it is only related to moving ice masses (see e.g. Benn and Evans, 2010). However, the presence of dead ice in the glacier forefield, as in the present case study, must be carefully considered for both water storage estimates and

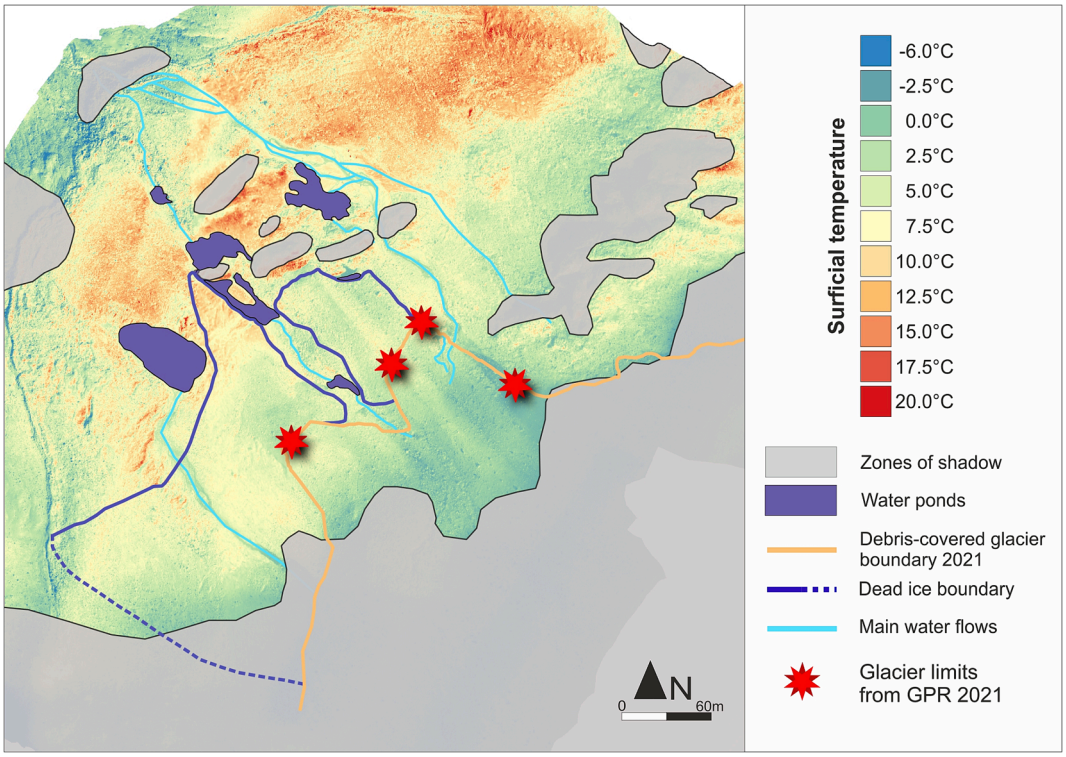

Fig. 7. Classified temperatures from 2021 UAV thermographic survey with some geomorphological features superimposed (see text for details).

in forecasts of future glacier evolution.

The range of surface temperatures of the debris covering dead-ice and the glacier is not different, therefore the utility of the thermal band is debated. Indeed, it is not possible to delineate the actual glacier terminus just on the basis of surface temperatures that change depending on the surface energy balance (i.e. albedo, aspect, slope, wind, surface moisture). However, thermal analysis still remains a valid technique to discriminate main domains within a glacial body (Forte et al., 2021).

In synthesis, no relevant correlations between dead ice patches location and elevation, retreat velocity, terrain slope, solar radiation, and surficial temperature have been found. Therefore, we concluded that the main factors possibly influencing the dead ice presence and thickness in the forefield of the Sforzellina Glacier are the morphology of the bedrock and the grain size of the debris. In particular, outcropping and deepening of the bedrock deduced from GPR survey seem to drive and favour dead ice patches occurrence. As shown in Fig. 3A, the rock top reflection deepens up to about 3 m just outside the actual glacier boundary, making such depression an optimal place for the preservation of ice during the glacier upward retreat. The same setting was identified in other locations where dead ice was detected. On the contrary, ridges in the bedrock morphology, corresponding for instance to the bedrock outcrops toward the North (Fig. 5) evidently cannot host dead ice patches. Moreover, Fig. 8 shows that the bedrock morphology is a relevant factor driving also the present glacier ice thickness and its internal facies distribution, in fact both bedrock depressions and ridges highly affect the glacial thickness, its dynamics and, as a consequence, the internal glaciological structures. For instance, in Fig. 8, shear zones are imaged in GPR profiles as high amplitude reflectors crossing the entire ice thickness, with a peculiar concave geometry. The shear zones geometry is clearly driven by the downward movement of the ice mass over an undulated bedrock morphology. In addition, shear zones represent a source of debris from the base of the glacier toward its surface. In fact, shear structures take charge of debris from the ground (basal) moraine releasing it close to or on the surface of the glacier, thus contributing to create, in a negative mass balance period, a denser debris cover on the glacier.

As far as the effect of debris thickness and size on dead ice preservation, while the fist parameter has a clear direct correlation as demonstrated by both field experiments, remote sensing analyses and laboratory measurements (e.g. Nakawo and Young, 1981; Zhang et al., 2011; Compagno et al., 2022, respectively), the second one has a more complex behaviour because supraglacial debris is typically not well-sorted and has variable hydraulic conductivity. In addition, rain and snowfalls have an important role in the ice isolation, but this topic is far from the aim of our study (Reznichenko et al., 2010).

Likely, with the progressive shrinking of the Sforzellina glacier expected in the next years, glacial ice would generally decrease its thickness and the glacier front would suffer a continuous retreating. If the debris cover keeps accumulating on the surface, other potential dead ice patches could probably form where, at present, the ice thickness is higher, being therefore more resilient to the glacier shrinking. This could most likely occur in correspondence to bedrock depressions (e.g. Fig. 8), with a dynamic balance between the progressive melting of the glacier ice and the consequent higher concentration of debris, which would insulate the ice, preserving it as dead ice for a certain time. With the present global warming conditions, such an evolution is expected for most of the alpine glaciers of the world, thus making more and more important to correctly estimate the actual glaciers boundary, even when they are (at least partially) covered by debris or snow and different outcropping and not outcropping glaciological units are present.

5. Conclusions

We demonstrated the effectiveness of the integration of GPR, geomorphological, and remote sensing data to assess the proper limit of a glacier, also highlighting the constraints arose. In fact, in glaciers ice is not always outcropping as it can be hidden by continuous debris cover, as well as by snow. Moreover, dead ice patches are not easily detectable through classical glaciological monitoring. GPR is essential for a proper characterization of different ice facies within the frozen body, namely clean ice, dirty ice, basal debris with ice, as well as dead ice patches all of

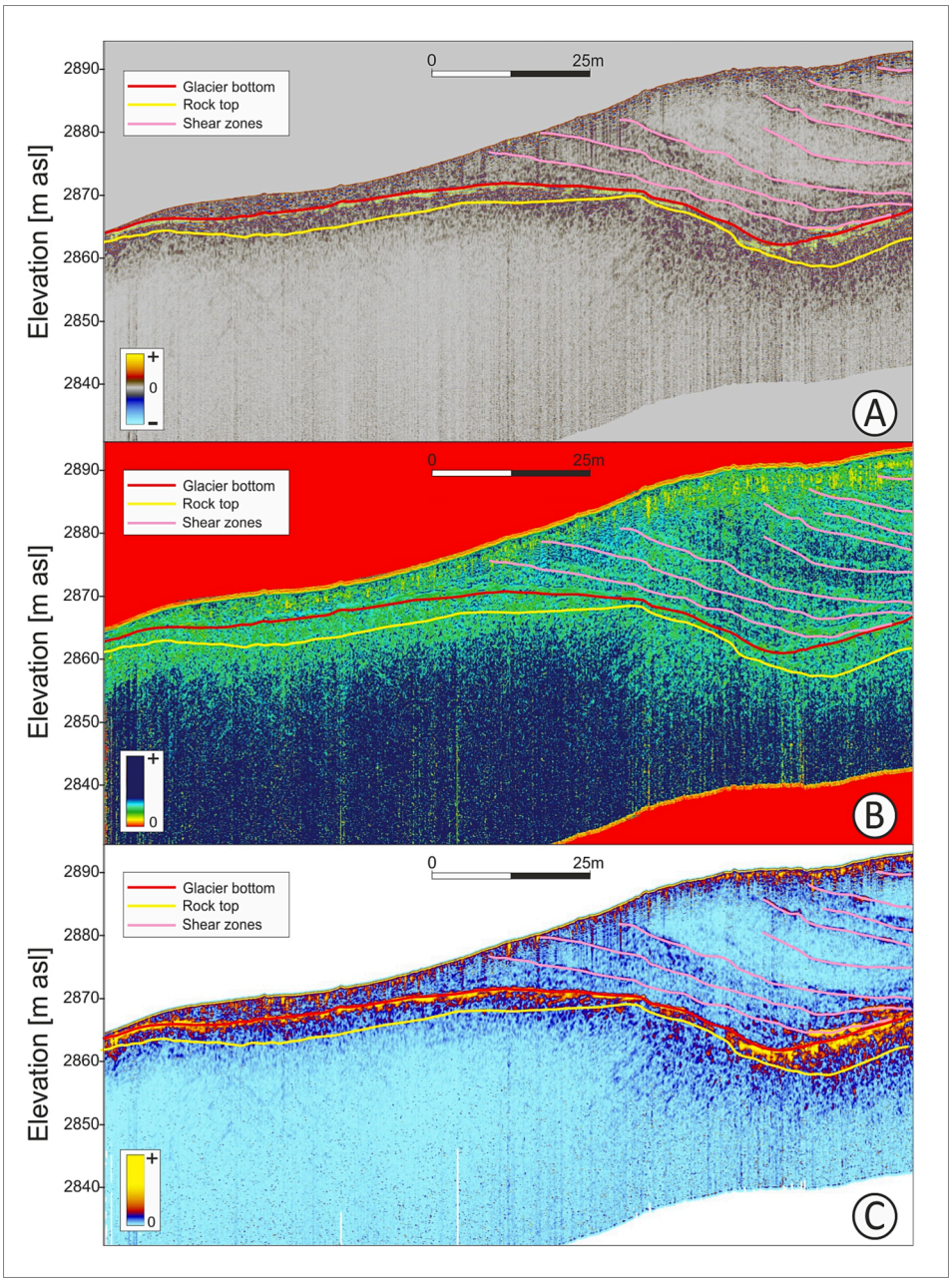

Fig. 8. Exemplary interpreted GPR profile across the glacier. Reflection amplitude (A); Dominant frequency (B); Sweetness attribute (C).

them having distinct and peculiar EM facies.

The presence of direct data allowed to calibrate the GPR dataset giving a physical meaning to the EM facies related to the *dead ice*. We found that the occurrence of dead ice patches is directly correlated to the bedrock morphology and specifically to its deepening, creating an optimal spot for the preservation of ice masses during glacier retreat phases. In addition, the documented accumulation of surficial debris creates the proper condition to dead ice preservation. On the other hand, we did not find relevant correlations between dead ice patches location and elevation, retreat velocity, terrain slope, solar radiation, and surficial temperature.

On the basis of the results obtained for the Sforzellina Glacier, we argue that estimates of glacier extensions just related to surficial information, like in the case of exclusive use of remote sensing data and outcropping ice monitoring, can produce relevant underestimations. The presence of hidden ice patches, which strictly speaking cannot be considered as a part of a glacier and is often undertaken, is indeed important to quantify the total water equivalent, as well as to make affordable forecasts of the future glaciers evolution.

Declaration of Competing Interest

The authors declare that they have no known competing financial interests or personal relationships that could have appeared to influence the work reported in this paper.

Acknowledgments

This research was partially funded by the Italian PNRA grant 18_00186-E Interactions between permafrost and ecosystems in Continental Antarctica–IPECA. We gratefully acknowledge Schlumberger for the University of Trieste Petrel® academic grant. Professor Adriano Ribolini and an anonymous reviewer are kindly acknowledged for their fruitful comments and suggestions.

References

Anderson, R.S., Anderson, L.S., Armstrong, W.H., Rossi, M.W., Crump, S.E., 2018. Glaciation of alpine valleys: The glacier – debris-covered glacier – rock glacier continuum. Geomorphology 311, 127–142. https://doi.org/10.1016/j.geomorph.2018.03.015.

Anderson, L.S., Anderson, R.S., 2016. Modelling debris-covered glaciers: response to steady debris deposition. Cryosphere 10, 1105–1124. https://doi.org/10.5194/tc-10-1105-2016.

Arcone, S.A., 1996. High resolution of glacial ice stratigraphy: a ground-penetrating radar study of Pegasus Runway, McMurdo Station, Antarctica. Geophysics 61, 1653–1663. https://doi.org/10.1190/1.1444084.

Benn, D.I., Evans, D.J.A., 2010. Glaciers and Glaciation. II edition, Hodder Education, p. 802.

Bernard, E., Friedt, J.M., Saintenoy, A., Tolle, F., Griselin, M., et al,2014. Where does a glacier end? GPR measurements to identify the limits between the slopes and the real glacier area. Application to the Austre Lovénbreen, Spitsbergen – 79°N. International Journal of Applied Earth Observation and Geoinformation, 27 (Part A), 100-108. doi: ff10.1016/j.jag.2013.07.006ff.

Bush, A.B.G., Bishop, M.P., Huo, D., Chi, Z., Tiwari, U., 2020. Issues in climate analysis and modelling for understanding mountain erosion dynamics. In: Reference Module in Earth Systems and Environmental Sciences. Elsevier), (Amsterdam). https://doi.org/10.1016/B978-0-12-818234-5.00022-5.

Cannone, N., Diolaiuti, G., Guglielmin, M., Smiraglia, C., 2008. Accelerating climate change impacts on alpine glacier forefield ecosystems in the European Alps. Ecol. Appl. 18, 637–648. https://doi.org/10.1890/07-1188.1.

Chopra, S., Marfurt, K.J., 2005. Seismic attributes — A historical perspective. Geophysics, 70, 3SO–28SO, doi: 10.1190/1.2098670.

Church, G., Bauder, A., Grab, M., Hansruedi, M., 2021. Ground-penetrating radar imaging reveals glacier's drainage network in 3D. The Cryosphere, 15, 3975–3988.

Colombero, C., Comina, C., De Toma, E., Franco, D., Godio, A., 2019. Ice Thickness Estimation from Geophysical Investigations on the Terminal Lobes of Belvedere Glacier (NW Italian Alps). Remote Sens. (Basel) 11, 805.

Compagno, L., Huss, M., Miles, E.S., McCarthy, M.J., Zekollari, H., Dehecq, A., Pellicciotti, F., Farinotti, D., 2022. Modelling supraglacial debris-cover evolution from the single-glacier to the regional scale: an application to High Mountain Asia. Cryosphere 16, 1697–1718. https://doi.org/10.5194/tc-16-1697-2022.

Dobreva, I.D., Bishop, M.P., Bush, A.B.G., 2017. Climate-glacier dynamics and topographic forcing in the Karakoram Himalaya: concepts, issues and research directions. Water 9, 405. https://doi.org/10.3390/w9060405.

Dossi, M., Forte, E., Pipan, M., 2015. Automated reflection picking and polarity assessment through attribute analysis: theory and application to synthetic and real GPR data. Geophysics 80, H23–H35. https://doi.org/10.1190/geo2015-0098.1.

Draebing, D., 2021. Identification of rock and fracture kinematics in high alpine rockwalls under the influence of elevation. Earth Surface Dynam. 9 (4), 977–994.

Ercoli, M., Pauselli, C., Cinti, F.R., Forte, E., Volpe, R., 2015. Imaging of an active fault: comparison between 3D GPR data and outcrops at the Castrovillari fault, Calabria, Italy. Interpretation, 3, 3, SY57–SY66, doi: 10.1190/INT-2014-0234.1.

Forte, E., Santin, I., Ponti, S., Colucci, R.R., Gutgesell, P., Guglielmin, M., 2021. New insights in glaciers characterization by differential diagnosis integrating GPR and remote sensing techniques: a case study for the Eastern Gran Zebrù glacier (Central Alps). Remote Sens. Environ. 267, 112715 https://doi.org/10.1016/j.rse.2021.112715.

Giese, A., Arcone, S., Hawley, R., Lewis, G., Wagnon, P., 2021. Detecting supraglacial debris thickness with GPR under suboptimal conditions. J. Glaciol. 67 (266), 1108–1120. https://doi.org/10.1017/jog.2021.59.

Godio, A., 2019. An overview on cryogeophysics in the Alpine environment. Bull. Geophys. Oceanogr. 61 (1), 3–22. https://doi.org/10.4430/bgta0304.

Godio, A., Rege, R.B., 2015. The mechanical properties of snow and ice of an alpine glacier inferred by integrating seismic and GPR methods. J. Appl. Geophys. 115, 92–99. https://doi.org/10.1016/j.jappgeo.2015.02.017.

Guglielmin, M., Nardo, A., Smiraglia, C., 1995. Lo spessore dei ghiacciai della Valfurva. Misurazioni tramite sondaggi elettrici verticali. Neve e Valanghe 24, 58–67 in Italian.

Henriksen, M., Mangerud, J., Matiouchkov, A., Paus, A., Svendsen, J.I., 2003. Lake stratigraphy implies an 80000 yr delayed melting of buried dead ice in northern Russia. J. Quat. Sci. 18 (7), 663–679. https://doi.org/10.1002/jqs.788.

Huo, D., Bishop, M.P., Bush, A.B.G., 2021. Understanding Complex Debris-Covered Glaciers: Concepts, Issues, and Research Directions. Front. Geosci. sec. Cryospheric Sci. https://doi.org/10.3389/feart.2021.652279.

Immerzeel, W.W., Van Beek, L.P., Bierkens, M.F., 2010. Climate change will affect the Asian water towers. Science 328, 1382–1385. https://doi.org/10.1126/science.1183188.

IPCC, 2021. Climate Change 2021: The Physical Science Basis. Contribution of Working Group I to the Sixth Assessment Report of the Intergovernmental Panel on Climate Change, Masson-Delmotte, V., P. Zhai, A. Pirani, S.L. Connors, et al. (eds.). Cambridge University Press, Cambridge, United Kingdom and New York, NY, USA, doi:10.1017/9781009157896.

Jol, H.M., 2009. Ground Penetrating Radar Theory and Application, first ed.,. Elsevier Science, p. 524 pp..

Kadioğlu, S., Kadioğlu, Y.K., 2016. Visualization of buried anti-tank landmines and soil pollution: analysis using ground penetrating radar method with attributes and petrographical methods. Near Surf. Geophys. 14 (2), 183–195. https://doi.org/10.3997/1873-0604.2016010.

Kraaijenbrink, P.D.A., Shea, J.M., Litt, M., Steiner, J.F., Treichler, D., Koch, I., Immerzeel, W.W., 2018. Mapping Surface Temperatures on a Debris-Covered Glacier With an Unmanned Aerial Vehicle. Front. Earth Sci. 6 https://doi.org/10.3389/feart.2018.0006.

Krüger, J., Kjær, K.H., Schomacker, A., 2010. Dead-Ice Environments: A land systems model for a debris-charged, stagnant lowland glacier margin. Kötlujökull. Dev. Quat. Sci. 13 (ISSN1571-0866), 105–127.

Lu, G., Zhao, W., Forte, E., Tian, G., Li, Y., Pipan, M., 2020. Multi-frequency and multi-attribute GPR data fusion based on 2-D wavelet transform. Measurement 166, 108243. https://doi.org/10.1016/j.measurement.2020.108243.

Mayr, E., Hagg, W., 2019. Debris-covered glaciers. In: Heckmann, T., Morche, D. (Eds.), Geomorphology of Proglacial Systems. Springer International Publishing, Cham, Landform and Sediment Dynamics in Recently Deglaciated Alpine Landscapes, pp. 59–71.

McClymont, A.F., Green, A.G., Streich, R., Horstmeyer, H., Tronicke, J., Nobes, D.C., Pettinga, J., Campbell, J., Langridge, R., 2008. Visualization of active faults using geometric attributes of 3D GPR data: an example from the Alpine Fault Zone. New Zealand. Geophysics 73 (2), B11–B23. https://doi.org/10.1190/1.2825408.

Montrasio, A., Berra, F., Cariboni, M., Ceriani, M., Deichmann, N., Ferliga, C., Gregnanin, A., Guerra, S., Guglielmin, M., Jadoul, F., Longhin, M., Mair, V., Mazzoccola, D., Sciesa, E., Zappone, A., 2012. Note illustrative della Carta Geologica d'Italia alla scala 1:50000 - foglio 024. ISPRA - Servizio Geologico d'Italia.

Nakawo, M., Young, G.J., 1981. Field experiments to determine the effect of a debris layer on ablation of glacier ice. Ann. Glaciol. 2, 85–91.

Navarro, F., Eisen, O., 2009. Ground-penetrating radar in glaciological applications. Rem. Sens. Glaciers 195–229. https://doi.org/10.1201/b10155-12.

Onaca, A.L., Gachev, E., Ardelean, F., Ardelean, A.C., Persoiu, A., Hegyi, A., 2022. Small is strong: Post-LIA resilience of Europe's Southernmost glaciers assessed by geophysical methods. Catena 213 (3), 106143. https://doi.org/10.1016/j.catena.2022.106143.

Paul, F., Huggel, C., Kääb, A., 2003. Combining satellite multispectral image data and a digital elevation model for mapping debris-covered glaciers. Remote Sens. Environ. 89 (4), 510–518. https://doi.org/10.1016/j.rse.2003.11.007.

Paul, F., Kääb, A., Haeberli, W., 2007. Recent glacier changes in the Alps observed by satellite: Consequences for future monitoring strategies. Global Planet. Change 56, 111–122. https://doi.org/10.1016/j.gloplacha.2006.07.007.

Paul, F., Barrand, N., Baumann, S., Berthier, E., Bolch, T., Casey, K., et al., 2013. On the accuracy of glacier outlines derived from remote-sensing data. Ann. Glaciol. 54 (63), 171–182. https://doi.org/10.3189/2013AoG63A296.

Paul, F., Rastner, P., Azzoni, R.S., Diolaiuti, G., Fugazza, D., Le Bris, R., Nemec, J., Rabatel, A., Ramusovic, M., Schwaizer, G., Smiraglia, C., 2019. Glacier inventory of the Alps from Sentinel-2, shape files. PANGAEA, doi: 10.1594/PANGAEA.909133.

Pipan, M., Baradello, L., Forte, E., Finetti, I., 2001. Ground penetrating radar study of iron age tombs in southeastern Kazakhstan. Archaeol. Prospect. 8, 141–155. https://doi.org/10.1002/arp.162.

Pavan, M., Diolaiuti, G., Smiraglia, C., Maggi, W., D'Agata, C., 2000. Prospezioni sismiche e radar sul Ghiacciaio della Sforzellina. Neve e Valanghe, 41. (in Italian).

Resnati, C., Smiraglia, C., 1989. Ghiacciaio dello Sforzellina – determinazione dello spessore del ghiacciaio tramite sondaggi geoelettrici. Club Alpino Italiano 110 (6), 70–75 in Italian.

Reznichenko, N., Davies, T., Shulmeister, J., McSaveney, M., 2010. Effects of debris on ice-surface melting rates: An experimental study. J. Glaciol. 56 (197), 384–394. https://doi.org/10.3189/002214310792447725.

Ribolini, A., Guglielmin, M., Fabre, D., Bodin, X., Marchisio, M., Sartini, S., Spagnolo, M., Schoeneich, P., 2010. The internal structure of rock glaciers and recently deglaciated slopes as revealed by geoelectrical tomography: insights on permafrost and recent glacial evolution in the Central and Western Alps (Italy–France), Quaternary Science Reviews, 29, 507-521, ISSN 0277-3791, doi: 10.1016/j.quascirev.2009.10.008.

Schomacker, A., 2007. Dead-Ice Under Different Climate Conditions: Processes, Landforms, Sediments and Melt Rates in Iceland and Svalbard. Quaternary Sciences, Department of Geology, Lund University, ISBN 978-91-86746-92-6.

Tarca, G., Guglielmin, M., 2022. Evolution of the sparse debris cover during the ablation season at two small Alpine glaciers (Gran Zebrù and Sforzellina, Ortles-Cevedale group). Geomorphology 409, 108268.

Yoshikawa, K., Leuschen, C., Ikeda, A., Harada, K., Gogineni, P., Hoekstra, P., Hinzman, L., Sawada, Y., Matsuoka, N., 2006. Comparison of geophysical investigations for detection of massive ground ice (pingo ice). J. Geophys. Res. 111, E06S19 https://doi.org/10.1029/2005JE002573.

Žebre, M., Colucci, R.R., Giorgi, F., Glasser, N.F., Racoviteanu, A.E., Del Gobbo, C., 2021. 200 years of equilibrium-line altitude variability across the European Alps (1901–2100). Clim. Dyn. 56, 1183–1201. https://doi.org/10.1007/s00382-020-05525-7.

Zhang, Y., Fujita, K., Liu, S., Liu, Q., Nuimura, T., 2011. Distribution of debris thickness and its effect on ice melt at Hailuogou glacier, southeastern Tibetan Plateau, using in situ surveys and ASTER imagery. J. Glaciol. 57 (206), 1147–1157. https://doi.org/10.3189/002214311798843331.

Zhao, W., Forte, E., Colucci, R.R., Pipan, M., 2016. High-resolution glacier imaging and characterization by means of GPR attribute analysis. Geophys. J. Int. 206, 1366–1374. https://doi.org/10.1093/gji/ggw208.

Zhao, W., Forte, E., Fontana, F., Pipan, M., Tian, G., 2018. GPR imaging and characterization of ancient Roman ruins in the Aquileia Archaeological Park, NE Italy. Measurement 113, 161–171. https://doi.org/10.1016/j.measurement.2017.09.004.